HHS Public Access

Author manuscript

Biochim Biophys Acta. Author manuscript; available in PMC 2017 February 11.

Structure of Decorin Binding Protein B from Borrelia burgdorferi and Its Interactions with Glycosaminoglycans

Wei Feng and **Xu Wang**

Department of Chemistry & Biochemistry, Arizona State University Tempe, AZ 85287

Abstract

Decorin-binding proteins (DBPs), DBPA and DBPB, are surface lipoproteins on *Borrelia burgdorferi*, causative agent of Lyme disease. DBPs bind to the connective tissue proteoglycan decorin and facilitate tissue colonization by the bacterium. Although structural and biochemical properties of DBPA are well understood, little is known about DBPB. In current work, we determined the solution structure of DBPB from strain B31 of *B. burgdorferi* and characterized its interactions with glycosaminoglycans (GAGs). Our structure shows DBPB adopts the same topology as DBPA, but possesses a much shorter terminal helix, resulting in a longer unstructured C-terminal tail, which is also rich in basic amino acids. Characterization of DBPB-GAG interactions reveals that, despite similar GAG affinities of DBPA and DBPB, the primary GAG-binding sites in DBPB are different from DBPA. In particular, our results indicate lysines in the C-terminus of DBPB are vital to DBPB's ability to bind GAGs whereas C-terminal tail for DBPA from strain B31 only plays a minor role in facilitating GAG bindings. Furthermore, the traditional GAG-binding pocket important to DBPA-GAG interactions is only secondary to DBPB's GAG-binding ability.

Graphical abstract

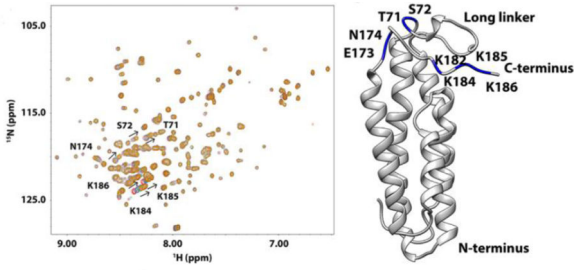

To whom correspondence should be addressed: Xu Wang, Department of Chemistry & Biochemistry, PSD-102, Arizona State University, Tempe, AZ 85287, USA. Telephone: (480)727-8256. Fax: (480)965-2747. xuwang@asu.edu.

ACCESSION NUMBER

Coordinates of the 10-structure DBPB ensemble are deposited in the PDB data bank with the accession number PDB: 2MVG. Atom chemical shift assignments of DBPB along with the constraints used to calculate the structure are deposited in the BioMagResBank with the accession number BMRB: 25266.

Keywords

Lyme disease; glycosaminoglycan; adhesin; NMR; decorin

Introduction

Borrelia burgdorferi is the causative agent of Lyme disease, which is the most prevalent vector-borne disease in North America. As an extracellular bacterium, *B. burgdorferi* relies almost entirely on host cells for nutrients. Because of its parasitic life cycle, *B. burgdorferi* has developed many strategies for adhering to and evading detection by the host. Many of the proteins involved in promoting the adhesion of the bacteria to the host cells have shown to be important to the virulence of the bacteria [1, 2]. Understanding the mechanisms of these virulent factors is therefore an important aspect in tackling *B. burgdorferi* infection.

One of the *B. burgdorferi* adhesins identified is decorin binding protein (DBP), a cell surface lipoprotein that is expressed during the mammalian infection stage [3]. Two homologous forms of DBP, termed DBPA and DBPB, exist in the *B. burgdorferi* genome. Both are lipoproteins of approximately 20 kDa in size, and they share ~ 40 % sequence identity. Genetic studies of the two isoforms show both are important for the bacteria during early stages of infection [4–6]. Although the two isoforms can compensate one another to a limited extent, absence of either one can produce defects in joint colonization and DBPB overexpression also inhibits proper dissemination of the bacterium [7, 8]. Interestingly, DBPA shows high sequence diversity among different strains of *Borrelia* bacteria, while DBPB sequence is well conserved [9–11].

DBPs facilitate bacterial colonization by adhering to proteoglycans in the extracellular matrix (ECM) and on cell surfaces. The ECM proteoglycan decorin is a particular important target for DBPs [3, 12], and the glycosaminoglycan (GAG) portion of decorin is a major binding site for the DBPs [13–15]. GAGs are sulfated linear polysaccharides composed of repeating disaccharide units of uronic acid and amino sugars [16]. Because of their high sulfation density and large size, GAGs have strong interactions with a number of extracellular proteins via electrostatic interactions. This enables them to act as receptors for signaling proteins and microbes. Although the GAG chains found in decorin are either chondroitin sulfate (CS) or dermatan sulfate (DS), which contain N-acetylgalactosamine (GalNAc) only, DBPs are also known to interact with other GAG types including heparin and heparan sulfate (HS), both of which contain glucosamine instead of GalNAc. In fact, DBPA's affinity for heparin is significantly higher than its affinity for DS [9, 13, 14, 17]. The core protein of decorin is also suspected to play a role in facilitating the interactions between decorin and DBPs [12, 13]. However, there is yet no evidence of direct interactions between the decorin core protein and DBPs.

Although DBPA has been extensively studied functionally and structurally [10, 13, 18, 19], very little information is available on DBPB. The lack of information is curious considering that one reason for the interest in DBPs is their potential as vaccine components. However, the high genetic diversity of DBPA means a single vaccine may not be sufficient in eliciting immunity against all strains of the bacterium. In this respect, DBPB, whose sequence is well

conserved among different strains, may be a better candidate for vaccine development. In fact, antibody against DBPB has been one of the most common antibodies found in serums of humans infected with the bacterium [20].

We have determined the solution structure of DBPB from strain B31 of *Borrelia burgdorferi* using solution NMR and characterized its interactions with GAGs. Structure of DBPB is homologous to the known DBPA structures. In particular, it is composed of five helices with an unstructured linker between helices one and two as well as a flexible C-terminal tail. However, the C-terminal helix of DBPB is considerably shorter than the helix in DBPA, resulting in a longer unstructured C-terminal tail that is enriched in basic amino acids. Characterizations of DBPB-GAG interactions showed DBPB has similar GAG affinities as DBPA, but possesses different binding sites than DBPA. In particular, although some of the lysine residues deemed important to DBPA's affinity for GAGs are also conserved in DBPB, the most important GAG-binding site in DBPB is its lysine-rich C-terminus, the elimination of which reduced the GAG affinity of DBPB significantly. These results indicate DBPB may be as important in facilitating bacterial adhesion as the well-studied DBPA.

Material and Methods

Expression and purification of B31 DBPB

The open reading frame (ORF) of the wild type (WT) B31 DBPB (residues 21–187) was synthesized by Genscript Inc. (Piscataway, NJ) and cloned into the pHUE vector with ORF of His-tagged ubiquitin at the 5' end [21]. Residue C21, which acts as the lipid anchor *in vivo*, was mutated to serine to prevent dimerization [3]. To construct DBPB mutants, the following forward primers were designed: K65S/K69S, 5'-GCGTTCACCGGCCTGAGCACGGGTAGCAGCGTTACCTCTGG-3'; R78S/K81S, 5'-GGCGGTCTGGCCCTGAGCGAAGCAAGCGTGCAGGCGATTG-3'; K81S, 5'-GGCCCTGCGCGAAGCAAGCGTGCAGGCGATTGTG-3'; K169S, 5'-GAAAGTGGTTAAAGAAAGCCAGAACATCGAAAACGG-3'; ^{184}SSSS^{187}, 5'-GGGCTCCGCGGTGGATCGAGC-3'; DBPB$_{21–183}$, 5'-GAAAAACAACAAAAGCTAAAAGAAAAAATGAAAG-3'. The reverse primers were designed: K65S/K69S, 5'-CCAGAGGTAACGCTGCTACCCGTGCTCAGGCCGGTGAACGC-3'; R78S/K81S, 5'-CAATCGCCTGCACGCTTGCTTCGCTCAGGGCCAGACCGCC-3' K81S, 5'-CAACAATCGCCTGCACGCTTGCTTCGCGCAGGGCC-3'; K169S, 5'-CCGTTTTCGATGTTCTGGCTTTCTTTAACCACTTTC-3'; ^{184}SSSS^{187} 5'-GGGAAGCTTTCAGCTGCTGCTGCTGCTTTTGTTGTTTTT-3'; DBPB$_{21–183}$, 5'-CTTTCATTTTTTCTTTTAGCTTTTGTTGTTTTTC-3'. The mutagenesis was done with the Agilent Quickchange site-directed mutagenesis kit according to the manufacturer's protocol, and confirmed by sequencing.

Escherichia coli BL21 (DE3) cells transformed with the expression vectors were grown in M9 medium at 37 °C to an OD$_{600}$ of 0.8. The cells were then induced with 0.5 mM IPTG before overnight incubation at 30 °C. $^{15}NH_4Cl$ and/or ^{13}C glucose were added into M9 medium for desired isotopic labeling. After cell harvesting by centrifugation, the resuspended cells were treated with 1 mg/mL lysozyme for 20 min and lysed via sonication.

After centrifugation, the supernatant was subjected to Ni-affinity chromatography with a 5 mL HisTrap column (GE Life Sciences). The bound DBPB was eluted from the column by applying an imidazole gradient of 35 to 500 mM at a flow rate of 3 mL/min. After exchanging the pooled protein into 25 mM Tris and 100 mM NaCl buffer (pH 8.0), the fusion protein was cleaved with 1/20 molar equivalent of USP2 (deubiquitinase) overnight at room temperature [21]. Another Ni-affinity chromatography was applied to separate cleaved DBPB from His-tagged ubiquitin and His-tagged USP2.

Production of GAG fragments and TEMPO-labeled GAG fragments

Heparin and DS from Sigma-Aldrich were partially depolymerized using heparinase I (IBEX Inc.) and chondroitinase ABC (Sigma-Aldrich), respectively [22, 23]. Digested fragments were separated based on size with a 2.5 cm × 175 cm size exclusion chromatography column (Bio-Rad Biogel P10) at a flow rate of 0.2 mL/min. Fractions containing fragments of the same size were pooled, desalted, and lyophilized. For paramagnetic relaxation enhancement (PRE) studies, DS dodecasaccharide, or dp12 (degree of polymerization 12) fragments were paramagnetically labeled by modifying the reducing end with the nitroxide radical, 4-amino-TEMPO, through reductive amination [19]. Specifically, 300 uM TEMPO was mixed with 1 mg of GAG fragments and 25 mM $NaCNBH_3$, and incubated at 65 °C for three days. After desalting, labeled fragments were further purified using SAX-HPLC.

Acquisition and analysis of NMR data for DBPB structure and backbone dynamics

NMR experiments were conducted on Bruker Ultra-Shield 600 MHz and Varian Inova 800 MHz spectrometers. Most of the pulse sequences were provided by the manufacturer. For backbone assignment, HNCACB, HNCOCACB, HNCO, and HNCOCA spectra were acquired for ^{13}C- and ^{15}N-labeled DBPB. To determine DBPB structure, ^{15}N- and ^{13}C-edited NOESY-HSQC spectra were obtained for ^{13}C- and ^{15}N-labeled DBPB. Methyl group assignments were made with the methyl HCCH-TOCSY experiments [24] while side chain proton assignments were made using a combination of HCCH-TOCSY, HCCONH and ^{13}C-edited NOESY-HSQC. HN and NC residual dipolar couplings (RDCs) were measured with DBPB aligned in a 7% neutral polyacrylamide gel using J-modulated pulse sequences [25]. NMR samples contain 100–600 uM of ^{13}C- and/or ^{15}N-labeled DBPB in 50 mM NaH_2PO_4 and 150 mM NaCl buffer (pH 6.5). All NMR data were processed with NMRPipe [26] and analyzed using NMRView [27].

For PRE studies, 400 uL of 150 uM WT ^{15}N-labeled DBPB was mixed with 8 molar equivalents of TEMPO-labeled DS dp12. PRE effect arising from the TEMPO-labeled fragments was estimated by collecting a ^{1}H-^{15}N HSQC spectrum before and after the radical was reduced by adding 3 uL of 1 M ascorbic acid [28].

To investigate the effects of GAG-binding on backbone mobility, backbone nitrogen T_1, T_2, and steady state heteronuclear nuclear Overhauser effect (NOE) were measured for WT ^{15}N-labeled DBPB with or without 10 molar equivalents of heparin dp10. Relaxation delays for longitudinal relaxation (T_1) and transverse relaxation (T_2) experiments were 0.1, 0.25, 0.4, 0.6, 0.8, 1.0 s and 10, 20, 40, 60, 80, 100 ms, respectively. Steady state heteronuclear NOE

was extracted by calculating peak intensity ratios of spectra collected with or without proton saturation of 3 s. The order parameter S^2 was calculated with the program relax [29] using the isotropic global rotational diffusion model. The global rotational correlation time, τ_m, was approximated as the average rotational correlation times of all structured residues. The residue-specific correlation times (τ_c) were determined according to the method of Kay et al [30]. Specifically, τ_c is estimated using the equation: $\tau_c = 1/(4(\pi\nu_N) \times [6(T_1/T_2) - 7]^{½}$, in which ν_N is the resonance frequency of ^{15}N in Hz. DS-induced millisecond time scale conformational exchange was measured on a sample containing 300 uM ^{15}N-labeled DBPB and 3 mM DS dp10 using the CPMG-based relaxation dispersion experiment designed by Tollinger et al [31]. The R_2 values were extracted by conducting two-point transverse relaxation measurements at relaxation delays of 5 and 50 ms. The field strength was varied from 10 to 210 Hz. The exchange component of the relaxation was estimated as the difference in R_2 values at field strengths of 10 and 210 Hz.

Structure calculation

Backbone dihedral angles of well-ordered residues were determined with the online server TALOS+ [32]. ^{13}C- and ^{15}N-edited NOESY-HSQC spectra were analyzed manually to find unambiguous long-range contacts. The partially assigned peak lists were then used as input for CYANA's automatic structure determination procedure [33]. The structures and constraint tables generated by CYANA were subsequently used in XPLOR-NIH for refinement with RDCs of HN and NC [34]. The 10 structures with the least NOE violations were shown as the ensemble in the present article.

Gel mobility shift assay

Heparin and DS fragments were fluorescently labeled with 2-aminoacridone (2-AMAC) according to the method of Lyon et al [35]. To confirm DBPB-GAG binding and size dependency of the interaction, 2 ug of 2-AMAC labeled heparin or DS fragments (dp4, dp6, dp8, and dp10) were incubated in 50 mM NaH_2PO_4 and 150 mM NaCl buffer (pH 6.5) containing 0 or 1 molar equivalent of WT DBPB. Gel mobility shift assays (GMSAs) were also carried out to compare the GAG binding affinities between DBPB and DBPA and between different mutants of DBPB. In these GMSAs, 1.5 ug of 2-AMAC heparin dp6 or DS dp10 was treated with 0, 0.5, and 1 molar equivalent of proteins. For all GMSAs, the mixtures were incubated at room temperature for 30 min and subjected to electrophoresis at 120 V for 15–25 min in 1% agarose gels made with 10 mM Tris-HCl, 1mM EDTA buffer (pH 6.4).

Affinity assay with immobilized GAGs

To compare the affinities of WT and mutant DBPBs for native GAGs, ELISA assays were performed with biotinylated heparin and DS immobilized on the neutravidin coated microwell plates (G-Biosciences). To prepare biotinylated GAGs, 550 ul reaction mixtures containing 1 mg of heparin or DS, 0.6 mM biotin, 2.5 mM EDC, 0.1 mM NHS and 100 mM MES (pH 5.5) were incubated overnight at room temperature and buffer exchanged to remove excess labels. For the ELISA, 2 ug of biotinylated heparin or DS was immobilized in each neutravidin well and probed with 2 ug of His-tagged WT DBPA, WT DBPB or mutant DBPBs. His-tagged ubiquitin was used as negative control. To detect bindings on all

ELISA assay plates, anti-HIS antibodies conjugated to horseradish peroxidase (HRP) from Qiagen were added. The assays were developed using tetramethylbenzidine (TMB) as the substrate and then quenched with 100 uL of 0.1 M HCl. Each ELISA was performed at least twice, and four replicates of each sample were analyzed to calculate average and standard deviation.

Titrations of DBPs with GAG fragments

For WT and mutant DBPBs titrations, aliquots of 5 mM heparin dp10 were added to 400 uL of 50 mM NaH_2PO_4 and 150 mM NaCl buffer (pH 6.5) containing 100 uM protein to reach final concentrations of 0.2, 0.6, 1.0, 1.4, 1.8, and 2.2 mM. A^1H-^{15}N HSQC spectrum was collected at each titration point. Chemical shift changes in ^1H and ^{15}N dimensions were combined to a single chemical shift value δ [36] using the equation $\delta = [\Delta\delta_H^2 + (2\Delta\delta_N)^2]^{1/2}$, with $\Delta\delta_H$ and $\Delta\delta_N$ representing the respective chemical shift changes in Hz on ^1H and ^{15}N dimensions. The Kds were determined using the 1:1 binding model in the software xcrvfit (http://www.bionmr.ualberta.ca/bds/software/xcrvfit/), which takes into consideration ligand depletion during the titration. Titrations of WT DBPB with heparin dp6 and DS dp10 were performed under the same conditions.

RESULTS

DBPB Structure

In this study, the structure of DBPB was determined using solution NMR methods. The ensemble of 10 DBPB structures most consistent with the experimental data is depicted in Figure 1. Table 1 shows the structural statistics for the ensemble. In agreement with the previous predictions, the solution structure of DBPB adopts a conformation very similar to the known DBPA structures [10, 18]. Specifically, DBPB consists of five helices as well as two flexible segments arranged similarly as DBPA. This topology brings the linker (residues 55–73) between helices one and two and the C-terminal tail in proximity. Extensive hydrophobic contacts between residues in helices two, three and five have been identified in NOESY, leading to the formation of the hydrophobic core that establishes the tertiary fold of the protein. Hydrogen/deuterium exchange experiments were also performed to measure the stability of the helices. Not surprisingly, backbone amide protons of residues in helices two, three and five showed the least hydrogen / deuterium exchange (data not shown), indicating the three helices are the most stable helices in the protein, consistent with their participation in the hydrophobic core.

Despite these similarities, DBPB differs from DBPA structurally in several respects. Figure 2 shows the sequence alignment of DBPA and DBPB from strain B31 of *B. burgdorferi* and positions of the helices in these proteins. The alignment reveals that secondary structural elements are well conserved between the two. However, the helical content of DBPB is lower than DBPA because helices one and five in DBPB are shorter than those in DBPA. Figure 3 is the superimposition of DBPA and DBPB structures. The helices of the two structures superimpose with a backbone RMSD of 2.0 Å. The superimposition shows that the positions of the helices are also conserved between the proteins, but shortening of helix five has resulted in a longer unstructured C-terminus in DBPB. Moreover, cysteines in the

C-terminal tail and helix five of DBPA form a disulfide bond that restrains the C-terminal tail to DBPA's core domain and reduces the tail's flexibility. However, such an intramolecular disulfide bond is missing in DBPB's C-terminus. Backbone dynamics experiments described below suggest the C-terminus as well as the linker between helices one and two are indeed very flexible. Another notable difference between B31 DBPA and DBPB is the lack of BXBB motif in the linker of DBPB. The BXBB motif in the linker has been shown to be an important GAG-binding site for GAGs in B31 DBPA[19]. The lack of a similar sequence in DBPB means the linker of DBPB may not play a role in GAG binding.

Because GAG-protein interactions are dominated by electrostatic attractions, electrostatic potential on the surface of the protein is predictive of possible GAG-binding sites. Figure 4 is the electrostatic potential map of DBPB. To avoid artifacts produced by the artificial cavity formed when the flexible segments are placed near the binding pocket, we removed the C-terminus and the linker between helices one and two and only calculated the electrostatic potential map of the core domains. A large basic patch can be seen in a pocket composed of helices two and five. A similar patch has also been observed in DBPA and was shown to be important in GAG binding [10, 37]. In agreement with the observation, the basic patch in DBPB includes residues K81 and K169, which are equivalent to two of the three GAG-binding residues identified in DBPA (Figure 2) [37].

Interactions of DBPB with GAGs

WT DBPB was analyzed in a series of experiments to characterize its GAG-binding properties. A qualitative examination using GMSA was carried out with WT DBPB and GAG fragments of defined sizes. In particular, fluorescently labeled heparin and DS tetrasaccharide (dp4), hexasaccharide (dp6), octasaccharide (dp8) and decasaccharide (dp10) were run on 1% agarose gel with or without DBPB. As shown in Figure 5, DBPB shifted a larger fraction of heparin fragments than DS fragments, indicating that DBPB binds heparin more strongly than DS. This is not unexpected considering the highly sulfated nature of heparin. The observations are also in line with previous studies using native long GAG chains, in which heparin was shown to be more effective in inhibiting bacterial adhesion than DS [14, 15].

To obtain more quantitative affinity estimates, we also carried out NMR-monitored titrations of DBPB using heparin and DS. As is often the case with GAG-binding proteins, long GAG chains induce protein oligomerization and lead to NMR signal broadening without revealing useful information on the GAG-binding residues. As a result, heparin dp10 and DS dp10 fragments were used in NMR analysis of DBPB-GAG interactions. Figure 6A shows ^{1}H-^{15}N HSQC spectra of DBPB titrated with heparin dp10 and Figure S1 shows the ^{1}H-^{15}N HSQC spectra of DBPB titrated with DS dp10. The amide proton and nitrogen chemical shift changes induced by both ligands are small compared to those seen in B31 DBPA [10]. Small chemical shift changes have been conventionally associated with multiple binding modes in protein-ligand interactions, which can reduce magnitudes of chemical shift changes as a result of chemical shift averaging between different binding conformations. Observations of these small chemical shift changes indicate DBPB-GAG interactions are less specific than DBPA-GAG interactions.

Using chemical shift changes from several residues that showed large perturbations, the dissociation constants (Kd) of the interaction were calculated for the titrations and the binding curves are shown in Figure 6 and Figure S1. The Kd of WT DBPB with heparin dp10 is in the 0.5 mM range. On the other hand, DS dp10 showed no sign of saturating the protein even at very high concentrations (Figure S1). This indicates DBPB's affinity for DS is weaker than heparin, which is consistent with the GMSA data. DS dp10 did induce broadening of many signals in the HSQC spectrum, suggesting that both affinity and kinetics of the interactions are different compared to heparin dp10. To confirm that signal broadening is the result of dynamic DBPB-DS interactions, we prepared a DBPB sample containing 10 molar equivalents of DS dp10 and measured the contribution of conformational exchange to transverse relaxation of amide nitrogen using CPMG-based NMR relaxation dispersion experiments [31]. The result of the CPMG experiments showed that most DS-induced relaxation dispersion can be refocused with a refocusing field strength less than 200 Hz, indicating interactions with DS occur on millisecond time scale. Moreover, the two residues that showed the strongest exchange relaxation are both located on the linker (G55 and T66) near the binding pocket (Figure S2). This is consistent with the hypothesis that signal broadening was induced by DS binding to the protein.

Because ligand-induced chemical shift perturbations can indicate the location of binding sites, we systematically tabulated heparin-induced chemical shift changes of backbone amide nitrogen and hydrogen for DBPB residues. Figure 6C shows ^{1}H-^{15}N chemical shift changes on a residue specific basis. The most perturbed residues were T71, S72, E173, N174, K182, K184, K185 and K186, most of which are located in the linker between helices one and two as well as the C- terminal tail, implying that those residues could be involved in GAG binding. Some residues showed unexpected signal intensity increase whereas the majority of residues had reduced peak intensities due to the dilution by heparin dp10 addition. The residues with increased intensities included G63, T66, K69, S72, G73, S183, K184, K185 and K186, which are also in the linker and the C-terminal tail. The increases in their signal intensities are most likely a result of GAG binding-induced reduction in the rate of backbone amide proton exchange with solvent. We also performed similar titrations of DBPB with heparin dp6 ligands to ensure the observed chemical shift patterns are not ligand size and composition dependent. The titration shows heparin dp6 ligands induced identical chemical shift change patterns in DBPB as heparin dp10 (Figure S3), confirming DBPB interacts with heparin dp6 in a similar manner as heparin dp10. However, Kd of interaction between DBPB and heparn dp6 was twice as large as the Kd of interaction between DBPB and heparin dp10. This is consistent with the conventional belief that longer heparin ligands have higher affinity for DBPB.

Unlike DS, signal broadening induced by heparin was minimal. This indicates interactions of heparin dp10 with DBPB fall in the fast exchange regime on the NMR time scale. However, because two flexible segments, the linker and the C-terminal tail, experienced substantial perturbations in chemical shift values upon binding GAGs, it is possible that GAG binding affects the nanosecond time scale motion of the two domains. To characterize the possible GAG-induced changes in conformational dynamics, we analyzed the dynamics of backbone amide nitrogens of the protein using the Lipari-Szabo model-free approach [38, 39]. This method represents the magnitude of internal rotational motions using the order

parameter S^2, whose values can be estimated with longitudinal relaxation rates, transverse relaxation rates and steady state heteronuclear NOE [30]. An S^2 of zero represents vigorous local motion while an S^2 of one represents complete rigidity. T_1, T_2 and ^1H-^{15}N NOE of the backbone amide nitrogen atoms were measured and fitted using the program relax [29] to obtain order parameters S^2 for these atoms. The data showed the long linker and the C-terminal tail are highly dynamic (Figure S4), but no significant change in order parameters was detected even after the addition of 10 molar equivalents of heparin dp10. These observations show heparin dp10 has no significant effects on DBPB's dynamics. Similar observations were also made for DBPA [19, 40]. Finally, although chemical shift mapping is the most popular technique for determining ligand-binding sites, artifacts can occur if protein undergoes significant conformation changes after binding the ligand. To unambiguously identify residues that are close to bound GAGs, we probed DBPB with DS dp12 ligands functionalized with the paramagnetic nitroxide radical TEMPO. The unpaired electron in the paramagnetic tag generates heterogeneous magnetic field and induces increased longitudinal and transverse relaxation rates of spins in the vicinity. The phenomenon, known as paramagnetic relaxation enhancement (PRE), leads to decreases in signal intensities of nearby residues in a distance-dependent manner such that atoms close to the paramagnetic center suffer greater loss of signal than atoms far away [41]. Figure 7A shows the overlays of ^1H-^{15}N HSQC spectra of a sample containing 0.15 mM WT B31 DBPB and 1.2 mM paramagnetic DS dp12 before and after the radical was reduced with ascorbic acid. The spectra revealed large increases in signal intensities of several residues upon the reduction of the radical, indicating that they are close to the paramagnetic center. These residues include L57, E59, G73, G74, Q83, I131, Q158, Q162, and N171. Figure 7B shows the location of these perturbed residues. Similar to the results of chemical shift perturbation analysis, most TEMPO-perturbed residues are also found in the linker, the C-terminus and the basic patch. This is direct evidence that those regions are involved in GAG binding.

Determination of DBPB's GAG-binding sites through mutagenesis

The DBPB structure identifies several possible GAG-binding sites. In order to study the contributions of these residues to GAG binding, WT and mutant DBPBs lacking one of the proposed sites were prepared and their heparin and DS affinities were measured. Previous studies suggested that three lysine residues (K82, K163 and K170) are crucial to the binding of DBPA with GAGs [18, 42]. As shown in Figure 2, only two of the residues (K81 and K169) are conserved in DBPB. However, DBPB contains an additional arginine residue at position 78, which is located on the same face of helix 2 as K81 and K169 and able to synergistically participate in GAG binding with these residues. Besides these basic amino acids, chemical shift mappings showed that two other lysines, K65 and K69 in the long linker of DBPB, experienced large perturbations upon GAG binding, implying that these two lysines are potentially critical to DBPB's GAG binding activity. Based on these observations, three mutants, K65S/K69S, R78S/K81S and K81S/K169S, were prepared. The fact that DBPB C-terminal tail is rich in lysines and is the most perturbed domain in chemical shift mapping implies that the C-terminal tail might be crucial to GAG binding. Therefore, mutants lacking the last four residues ($DBPB_{21–183}$) or having them mutated from lysines to serines ($^{184}SSSS^{187}$) were also prepared.

To evaluate the contributions of the proposed sites to GAG bindings, the GAG affinities of the mutants were characterized with NMR-monitored titrations, GMSA and ELISA. First, we measured different DBPB mutants' affinities for intact heparin and DS using ELISA assays with immobilized heparin and DS. As shown in Figure 8, the assays revealed the interactions of all mutants with native GAG chains were severely diminished. These results confirm the basic amino acids identified are crucial to GAG binding. We also studied the effect of the mutations on DBPB's interactions with sized-defined GAG fragments using GMSA and NMR. Results of the GMSA are shown in Figure 9. In the assay, WT DBPB shifted almost all heparin dp6 fragments. In contrast, the two C-terminus mutants failed to shift any GAG fragments while R78S/K81S and K81S/K169S mutants induced shifts of only a small fraction of GAGs. K65S/K69S induced a significant amount of fragment migration, but the fraction of the shifted fragments was still much less than that of the WT DBPB. Similar results were obtained using a DS-based GMSA (Figure 9). These results are in qualitative agreement with the ELISA data, and show K65 and K69 are not as important as other clusters of basic amino acids. Quantitative evaluations of binding affinities were also carried out by titrating the mutants with heparin dp10 (Figures S5 & S6). The dissociation constants (Kd) derived from the titrations are shown in Table 2. The Kds are consistent with the result of GMSA in Figure 9. Specifically, WT DBPB's Kd is smaller than all mutants, while the Kds of K65S/K69S, R78S/K81S and K81S/K169S mutants all showed varying degrees of increase compared to the WT protein. In contrast, two C-terminal mutants, ^{184}SSSS^{187} and DBPB$_{21–183}$, showed no significant chemical shift migrations, suggesting their GAG affinities are severely attenuated (Figures S5D and S5E). Based on the results, we believe that the last four lysine residues are the most important GAG binding site in DBPB.

GAG affinity comparisons between DBPA and DBPB

To determine whether there are differences in GAG affinities of DBPA and DBPB, we probed their interactions with intact long chains of heparin and DS using ELISA. Our data showed B31 versions of DBPA and DBPB have similar affinities for both heparin and DS in ELISA (Figure S7A). This shows DBPB can be as important a GAG adhesin as DBPA. GMSA assay carried out on B31 DBPA and DBPB using size defined heparin dp6 also confirmed the similarities in their GAG affinities (Figure S7B).

DISCUSSION

In this work, we determined the solution structure of DBPB from strain B31 of *B. burgdorferi* and determined its GAG binding residues. The topology of DBPB is similar to that of DBPA. Both have five helices and two unstructured segments [10, 18]. Despite the similarities, their structures differ in several significant ways. Specifically, the C-terminal helix of DBPB is shorter than the corresponding helix in DBPA, leading to a far longer C-terminal tail that is unrestricted by any disulfide bond. The C-terminus is also distinguished from its DBPA counterpart by the large number of lysines found at its end. Most results from this study indicate these C-terminal basic residues contribute significantly to the GAG affinity of DBPB. In particular, the C-terminal residues (K184, K185 and K186) showed the largest changes in chemical shifts when DBPB was titrated with heparin dp10 and heparin

dp6 (Figures 6 and S3). Removing the last four residues or mutating them to serine also attenuated DBPB's affinity greatly. All these show the C-terminus is an important GAG-binding site in DBPB. Although B31 DBPA did have two basic residues close to its C-terminus, previous study indicated that their impact on GAG affinity of DBPA was modest [19]. We believe the location of these basic amino acids (none are located at the very terminus) in DBPA and the presence of the disulfide bond in DBPA may have restricted GAG ligands' access to the C-terminus of B31 DBPA. However, DBPA sequence heterogeneity is large, and C-termini of DBPAs from strain VS461 of *Borrelia afzelii* and strain PBr of *Borrelia garinii* have been shown to play a crucial role in their GAG binding activity [13, 40], setting the precedence for the involvement of C-termini in GAG binding. What is different between DBPB and all versions of DBPA studied so far is that the canonical GAG binding site made up of basic amino acids from helices 2 and 5 do not appear to contribute as much to GAG binding in DBPB as it did in DBPA. This might be because the number of basic amino acids in DBPB's canonical GAG-binding pocket is half that of DBPA. In particular, both K163 and R166 of B31 DBPA do not have equivalent basic residues in DBPB. The fact that the BXBB motif found in the linker of B31 DBPA is also missing in DBPB means the linker cannot contribute to GAG binding either. This may have further accentuated the importance of C-terminus of DBPB in GAG binding.

The flexible nature of the C-terminus means GAG's interaction with the C-terminus most likely lacks precise geometric constraints and multiple binding conformations are possible. This is consistent with the PRE-perturbation data, which showed the reducing end of the ligand can be located in several locations. It also agrees with the smaller heparin-induced chemical shift perturbations observed for DBPB since heterogeneity in binding conformation are believed to reduce the magnitudes of chemical shift perturbations.

Of the five mutants investigated for their GAG-binding activity, all showed lower GAG affinities than WT DBPB. In particular, K65S/K69S, R78S/K81S and K81S/K169S mutants exhibited significant decreases in their affinities for both heparin and DS size-defined ligands, while $DBPB_{21–183}$ and $^{184}SSSS^{187}$ mutants showed no binding to these short GAG fragments. These data indicate that all three clusters play a role in promoting GAG binding, but the C-terminus is especially critical. Interestingly, in the ELISA assay, the $^{184}SSSS^{187}$ mutant showed slightly higher binding for native GAG polysaccharides than the $DBPB_{21–183}$ mutant. It is possible that serines at the C-terminal tail are capable of mediating minor GAG binding through hydrogen bond interactions, while the truncation of the C-terminus completely attenuates the interaction. One factor that could have enhanced the importance of the C-terminus in GAG binding may be its accessibility to ligands. Specifically, although dynamic, the location of linker means it can still pose a significant barrier to interactions between GAGs and the basic pocket. The surface exposed nature of the C-terminus means it is more likely to interact with GAGs than basic residues in the pocket, therefore exerts a strong influence on GAG affinity of the protein. In fact, B31 DBPB is not the only DBP with important GAG-binding in its C-terminus. The C-terminus of DBPA from *Borrelia afzelii* strain VS461 is also crucial to the protein's GAG affinity [13]. Despite its importance in facilitating GAG-binding, the C-terminal tail showed no sign of perturbation in the PRE experiment. We believe this is possible because only the reducing

end of DS dp12 is labeled with TEMPO, and the C-terminal tail may interact mainly with the non-reducing ends of the GAG fragments, allowing it to be unaffected by the paramagnetic tag.

Supplementary Material

Refer to Web version on PubMed Central for supplementary material.

ACKNOWLEDGEMENTS

We want to thank Dr. Brian Cherry of ASU Magnetic Resonance Research Center for maintaining the spectrometers used in this study. Funding for this study was provided by National Institute of General Medical Sciences (R00GM088483) and Arizona State University.

REFERENCES

1. Brissette CA, Gaultney RA. That's my story, and I'm sticking to it--an update on B. burgdorferi adhesins. Front Cell Infect Microbiol. 2014; 4:41. [PubMed: 24772392]
2. Coburn J, Leong J, Chaconas G. Illuminating the roles of the Borrelia burgdorferi adhesins. Trends Microbiol. 2013; 21:372–379. [PubMed: 23876218]
3. Guo BP, Brown EL, Dorward DW, Rosenberg LC, Hook M. Decorin-binding adhesins from Borrelia burgdorferi. Molecular microbiology. 1998; 30:711–723. [PubMed: 10094620]
4. Shi Y, Xu Q, McShan K, Liang FT. Both decorin-binding proteins A and B are critical for the overall virulence of Borrelia burgdorferi. Infection and immunity. 2008; 76:1239–1246. [PubMed: 18195034]
5. Weening EH, Parveen N, Trzeciakowski JP, Leong JM, Hoeoek M, Skare JT. Borrelia burgdorferi Lacking DbpBA Exhibits an Early Survival Defect during Experimental Infection. Infection and immunity. 2008; 76:5694–5705. [PubMed: 18809667]
6. Imai DM, Samuels DS, Feng S, Hodzic E, Olsen K, Barthold SW. The early dissemination defect attributed to disruption of decorin-binding proteins is abolished in chronic murine lyme borreliosis. Infect Immun. 2013; 81:1663–1673. [PubMed: 23460518]
7. Salo J, Jaatinen A, Soderstrom M, Viljanen MK, Hytonen J. Decorin Binding Proteins of Borrelia burgdorferi Promote Arthritis Development and Joint Specific Post-Treatment DNA Persistence in Mice. PLoS One. 2015; 10:e0121512. [PubMed: 25816291]
8. Shi Y, Xu Q, Seemanaplli SV, McShan K, Liang FT. Common and unique contributions of decorin-binding proteins A and B to the overall virulence of Borrelia burgdorferi. PloS one. 2008; 3:e3340. [PubMed: 18833332]
9. Fischer JR, Parveen N, Magoun L, Leong JM. Decorin-binding proteins A and B confer distinct mammalian cell type-specific attachment by Borrelia burgdorferi the Lyme disease spirochete. Proceedings of the National Academy of Sciences of the United States of America. 2003; 100:7307–7312. [PubMed: 12773620]
10. Wang X. Solution structure of decorin-binding protein A from Borrelia burgdorferi. Biochemistry. 2012; 51:8353–8362. [PubMed: 22985470]
11. Roberts WC, Mullikin BA, Lathigra R, Hanson MS. Molecular analysis of sequence heterogeneity among genes encoding decorin binding proteins A and B of Borrelia burgdorferi sensu lato. Infection and immunity. 1998; 66:5275–5285. [PubMed: 9784533]
12. Guo BP, Norris SJ, Rosenberg LC, Hook M. Adherence of Borrelia burgdorferi to the proteoglycan decorin. Infection and immunity. 1995; 63:3467–3472. [PubMed: 7642279]
13. Benoit VM, Fischer JR, Lin YP, Parveen N, Leong JM. Allelic variation of the Lyme disease spirochete adhesin DbpA influences spirochetal binding to decorin dermatan sulfate and mammalian cells. Infection and immunity. 2011; 79:3501–3509. [PubMed: 21708995]

14. Leong JM, Robbins D, Rosenfeld L, Lahiri B, Parveen N. Structural requirements for glycosaminoglycan recognition by the Lyme disease spirochete Borrelia burgdorferi. Infection and immunity. 1998; 66:6045–6048. [PubMed: 9826395]
15. Parveen N, Robbins D, Leong JM. Strain variation in glycosaminoglycan recognition influences cell-type-specific binding by lyme disease spirochetes. Infect Immun. 1999; 67:1743–1749. [PubMed: 10085013]
16. Varki, A. Essentials of glycobiology. 2nd ed.. Cold Spring Harbor, N.Y.: Cold Spring Harbor Laboratory Press; 2009.
17. Leong JM, Wang H, Magoun L, Field JA, Morrissey PE, Robbins D, Tatro JB, Coburn J, Parveen N. Different classes of proteoglycans contribute to the attachment of Borrelia burgdorferi to cultured endothelial and brain cells. Infection and immunity. 1998; 66:994–999. [PubMed: 9488387]
18. Fortune DE, Lin YP, Deka RK, Groshong AM, Moore BP, Hagman KE, Leong JM, Tomchick DR, Blevins JS. Identification of Lysine Residues in the Borrelia burgdorferi DbpA Adhesin Required for Murine Infection. Infection and immunity. 2014
19. Morgan A, Wang X. The novel heparin-binding motif in decorin-binding protein A from strain B31 of Borrelia burgdorferi explains the higher binding affinity. Biochemistry. 2013; 52:8237–8245. [PubMed: 24148022]
20. Barbour AG, Jasinskas A, Kayala MA, Davies DH, Steere AC, Baldi P, Felgner PL. A genome-wide proteome array reveals a limited set of immunogens in natural infections of humans and white-footed mice with Borrelia burgdorferi. Infect Immun. 2008; 76:3374–3389. [PubMed: 18474646]
21. Catanzariti AM, Soboleva TA, Jans DA, Board PG, Baker RT. An efficient system for high-level expression and easy purification of authentic recombinant proteins. Protein Sci. 2004; 13:1331–1339. [PubMed: 15096636]
22. Xiao Z, Zhao W, Yang B, Zhang Z, Guan H, Linhardt RJ. Heparinase 1 selectivity for the 3,6-di-O-sulfo-2-deoxy-2-sulfamido-alpha-D-glucopyranose (1,4) 2-O-sulfo-alpha-L-idopyranosyluronic acid (GlcNS3S6S–IdoA2S) linkages. Glycobiology. 2011; 21:13–22. [PubMed: 20729345]
23. Yang HO, Gunay NS, Toida T, Kuberan B, Yu G, Kim YS, Linhardt RJ. Preparation and structural determination of dermatan sulfate-derived oligosaccharides. Glycobiology. 2000; 10:1033–1039. [PubMed: 11030749]
24. Wurtz P, Hellman M, Tossavainen H, Permi P. Towards unambiguous assignment of methyl-containing residues by double and triple sensitivity-enhanced HCCmHm-TOCSY experiments. J Biomol Nmr. 2006; 36:13–26. [PubMed: 16964533]
25. Liu Y, Prestegard JH. Measurement of one and two bond N-C couplings in large proteins by TROSY-based J-modulation experiments. J Magn Reson. 2009; 200:109–118. [PubMed: 19581113]
26. Delaglio F, Grzesiek S, Vuister GW, Zhu G, Pfeifer J, Bax A. NMRPipe: a multidimensional spectral processing system based on UNIX pipes. Journal of biomolecular NMR. 1995; 6:277–293. [PubMed: 8520220]
27. Johnson BA. Using NMRView to visualize and analyze the NMR spectra of macromolecules. Methods Mol Biol. 2004; 278:313–352. [PubMed: 15318002]
28. Iwahara J, Tang C, Marius Clore G. Practical aspects of (1)H transverse paramagnetic relaxation enhancement measurements on macromolecules. J Magn Reson. 2007; 184:185–195. [PubMed: 17084097]
29. d'Auvergne EJ, Gooley PR. Optimisation of NMR dynamic models I. Minimisation algorithms and their performance within the model-free and Brownian rotational diffusion spaces. Journal of biomolecular NMR. 2008; 40:107–119. [PubMed: 18085410]
30. Kay LE, Torchia DA, Bax A. Backbone dynamics of proteins as studied by 15N inverse detected heteronuclear NMR spectroscopy: application to staphylococcal nuclease. Biochemistry. 1989; 28:8972–8979. [PubMed: 2690953]
31. Tollinger M, Skrynnikov NR, Mulder FA, Forman-Kay JD, Kay LE. Slow dynamics in folded and unfolded states of an SH3 domain. J Am Chem Soc. 2001; 123:11341–11352. [PubMed: 11707108]

32. Shen Y, Delaglio F, Cornilescu G, Bax A. TALOS+: a hybrid method for predicting protein backbone torsion angles from NMR chemical shifts. Journal of biomolecular NMR. 2009; 44:213–223. [PubMed: 19548092]

33. Guntert P. Automated NMR structure calculation with CYANA. Methods Mol Biol. 2004; 278:353–378. [PubMed: 15318003]

34. Schwieters CD, Kuszewski JJ, Tjandra N, Clore GM. The Xplor-NIH NMR molecular structure determination package. J Magn Reson. 2003; 160:65–73. [PubMed: 12565051]

35. Lyon M, Deakin JA, Lietha D, Gherardi E, Gallagher JT. The interactions of hepatocyte growth factor/scatter factor and its NK1 and NK2 variants with glycosaminoglycans using a modified gel mobility shift assay. Elucidation of the minimal size of binding and activatory oligosaccharides. The Journal of biological chemistry. 2004; 279:43560–43567. [PubMed: 15292253]

36. Farmer BT 2nd, Constantine KL, Goldfarb V, Friedrichs MS, Wittekind M, Yanchunas J Jr, Robertson JG, Mueller L. Localizing the NADP+ binding site on the MurB enzyme by NMR. Nat Struct Biol. 1996; 3:995–997. [PubMed: 8946851]

37. Pikas DS, Brown EL, Gurusiddappa S, Lee LY, Xu Y, Hook M. Decorin-binding sites in the adhesin DbpA from Borrelia burgdorferi: a synthetic peptide approach. The Journal of biological chemistry. 2003; 278:30920–30926. [PubMed: 12761224]

38. Lipari G, Szabo A. Model-Free Approach to the Interpretation of Nuclear Magnetic-Resonance Relaxation in Macromolecules .1. Theory and Range of Validity. Journal of the American Chemical Society. 1982; 104:4546–4559.

39. Lipari G, Szabo A. Model-Free Approach to the Interpretation of Nuclear Magnetic-Resonance Relaxation in Macromolecules .2. Analysis of Experimental Results. Journal of the American Chemical Society. 1982; 104:4559–4570.

40. Morgan AM, Wang X. Structural mechanisms underlying sequence-dependent variations in GAG affinities of decorin binding protein A, a Borrelia burgdorferi adhesin. Biochem J. 2015; 467:439–451. [PubMed: 25695518]

41. Bertini, I.; Luchinat, C.; Parigi, G. Solution NMR of Paramagnetic Molecules: Applications to metallobiomolecules and models. 2 ed.. Elsevier Science; 2001.

42. Brown EL, Guo BP, O'Neal P, Hook M. Adherence of Borrelia burgdorferi. Identification of critical lysine residues in DbpA required for decorin binding. The Journal of biological chemistry. 1999; 274:26272–26278. [PubMed: 10473582]

Highlights

- Structure of DBPB is homologous to DBPA.
- GAG-binding sites of DBPB differ from that of DBPA.
- The C-terminus of DBPB is a significant GAG-binding site.
- DBPB's interaction with GAGs is most likely less specific than that of DBPA.

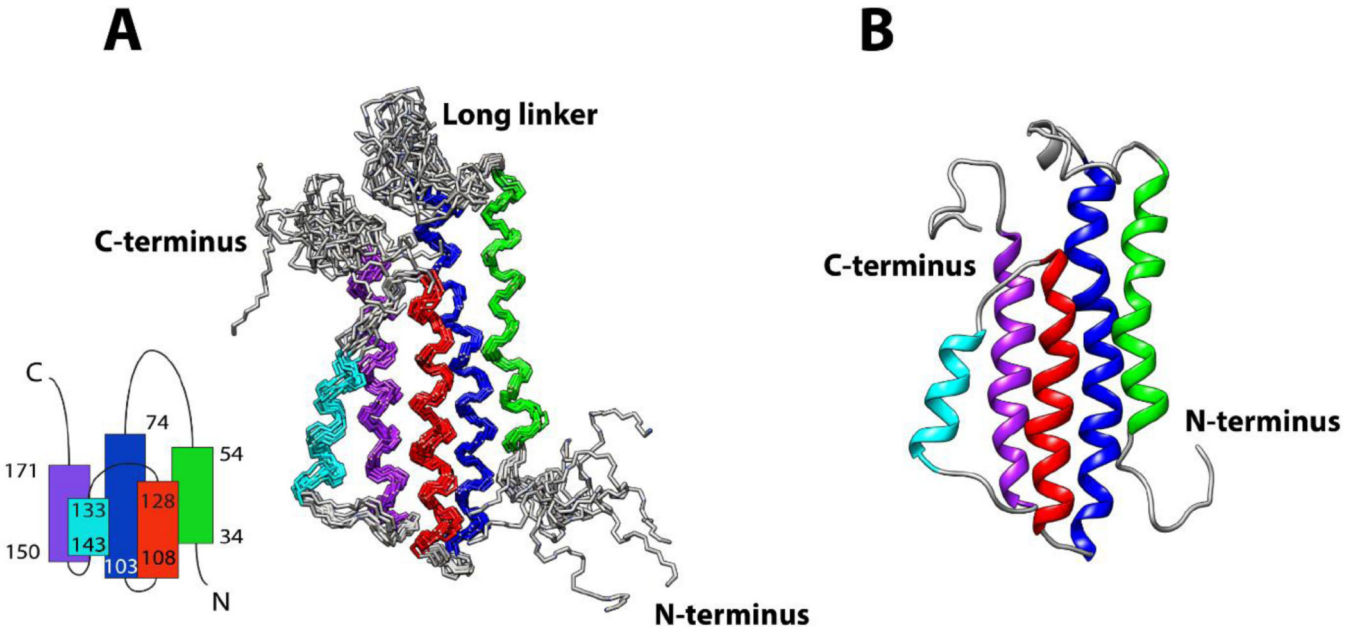

Figure 1. Solution structures of DBPB

(A) Ensemble of the 10 lowest-energy DBPB structures. Helix 1, consisting of residues 34 to 54, is colored green. Helix 2, consisting of residues 74 to 103, is colored blue. Helix 3, consisting of residues 108 to 128, is colored red. Helix 4, consisting of residues 133 to 143, is colored cyan. Helix 5, consisting of residues 150 to 171, is colored purple. The topology of DBPB is shown at the bottom left. (B) Ribbon depiction of a representative DBPB structure.

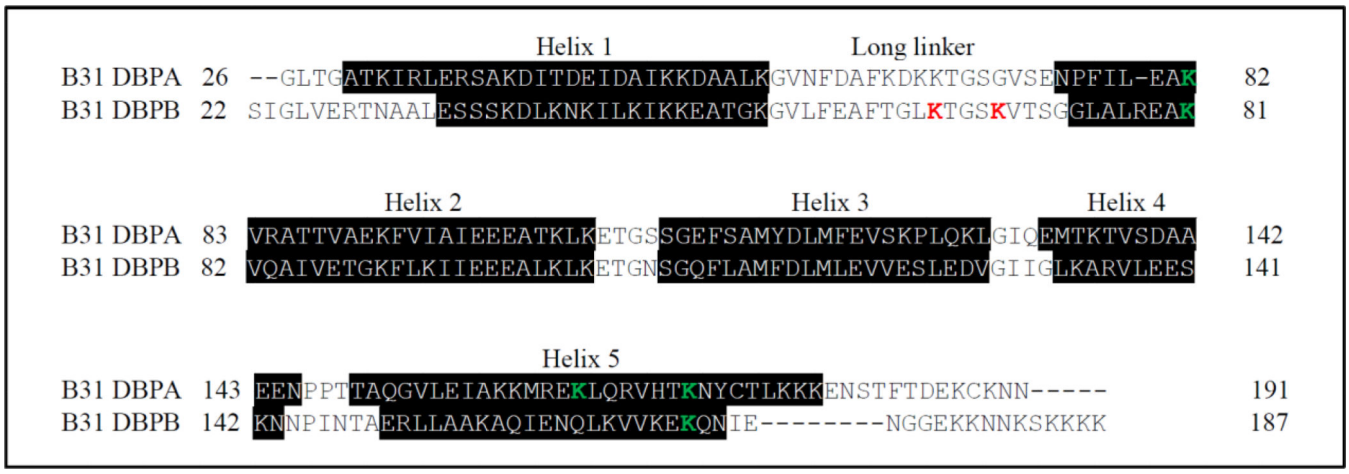

Figure 2. Sequence alignment of B31 DBPA and B31 DBPB

Lipidation signals of the proteins are not shown. Secondary structures are labeled with helices in black boxes. K82, K163 and K170 are colored green in DBPA. K65 and K69 are colored red, while conserved K81 and K169 are colored green in DBPB.

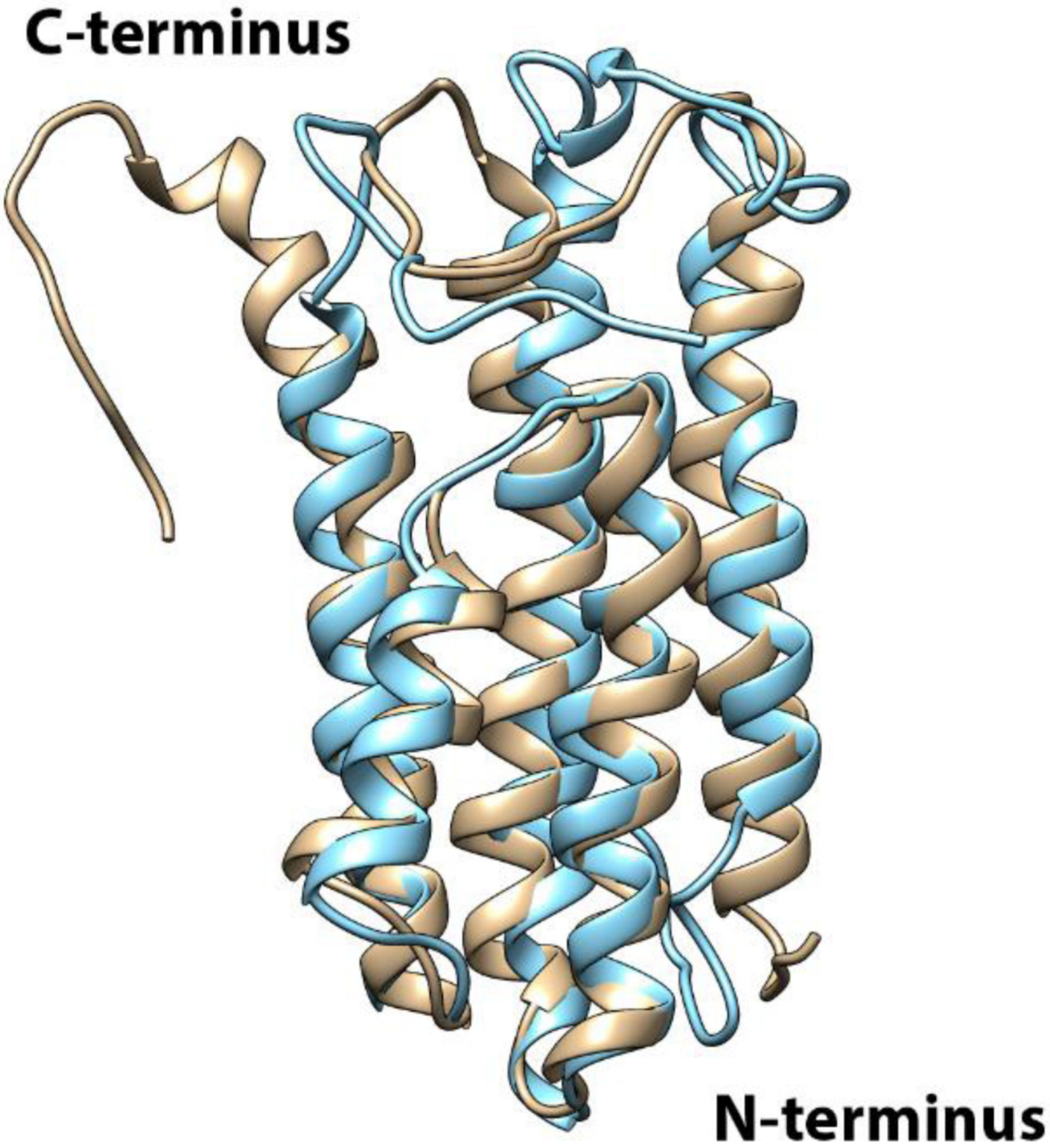

Figure 3. Superimposition of B31 DBPA and B31 DBPB structures

Ribbon representation of DBPA (PDB #2LQU) is shown in gold and ribbon representation of DBPB is shown in cyan.

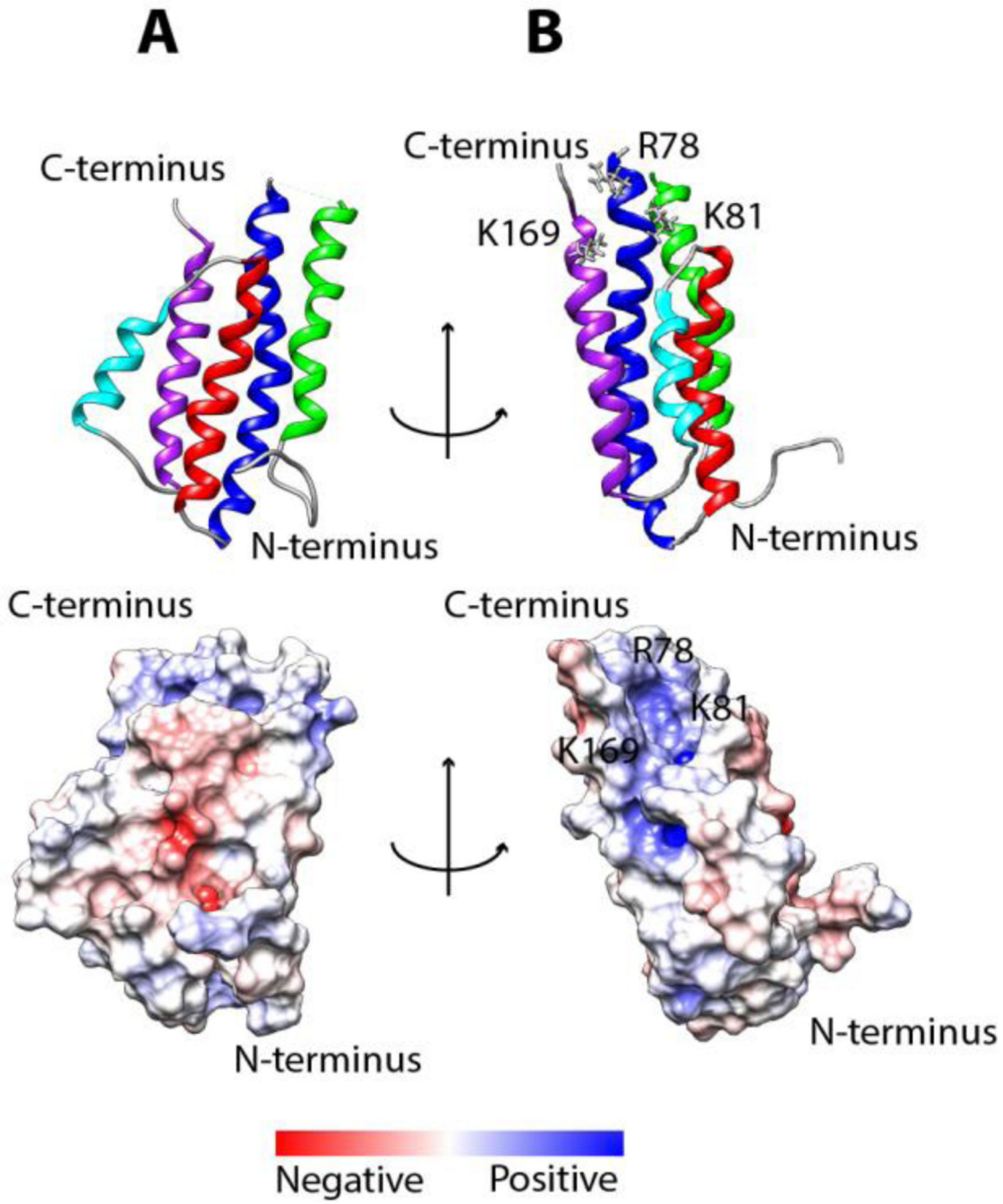

Figure 4. Electrostatic potential surface map of DBPB

Calculation of the surface electrostatic potential was carried out without the flexible linker and the C-terminal tail. (A) DBPB is in the same orientation as Figure 1B. (B) DBPB is rotated by 90 degrees about the vertical axis. R78, K81 and K169 are outlined.

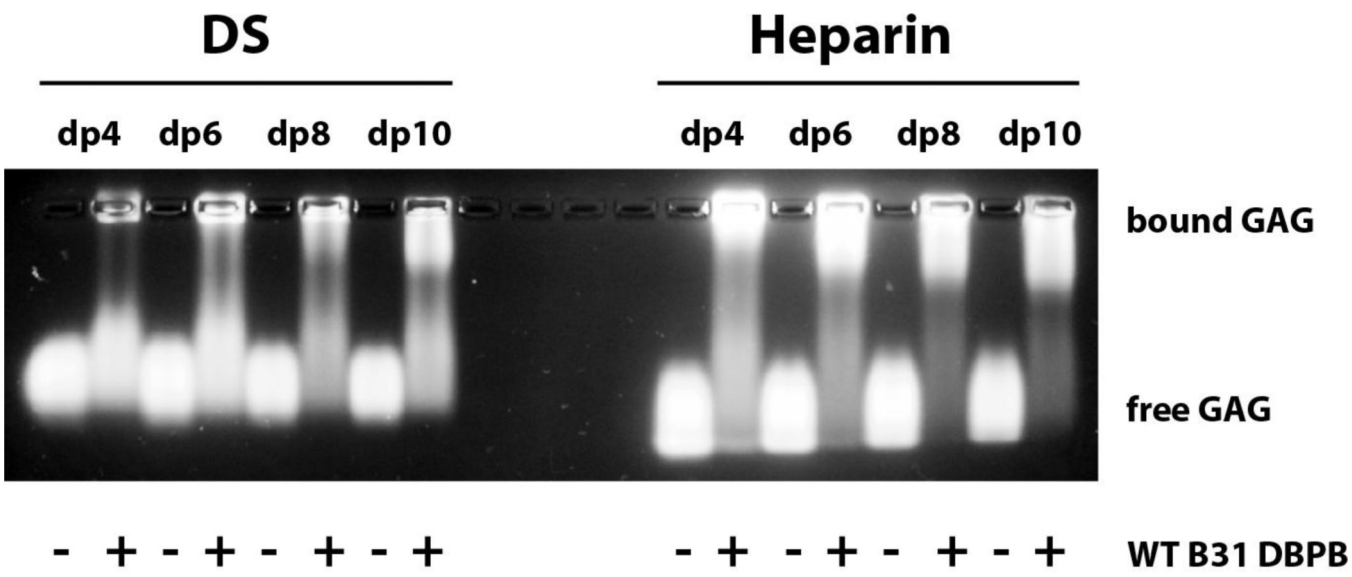

Figure 5. Gel mobility shift assay evaluation of WT DBPB's interactions with heparin and DS

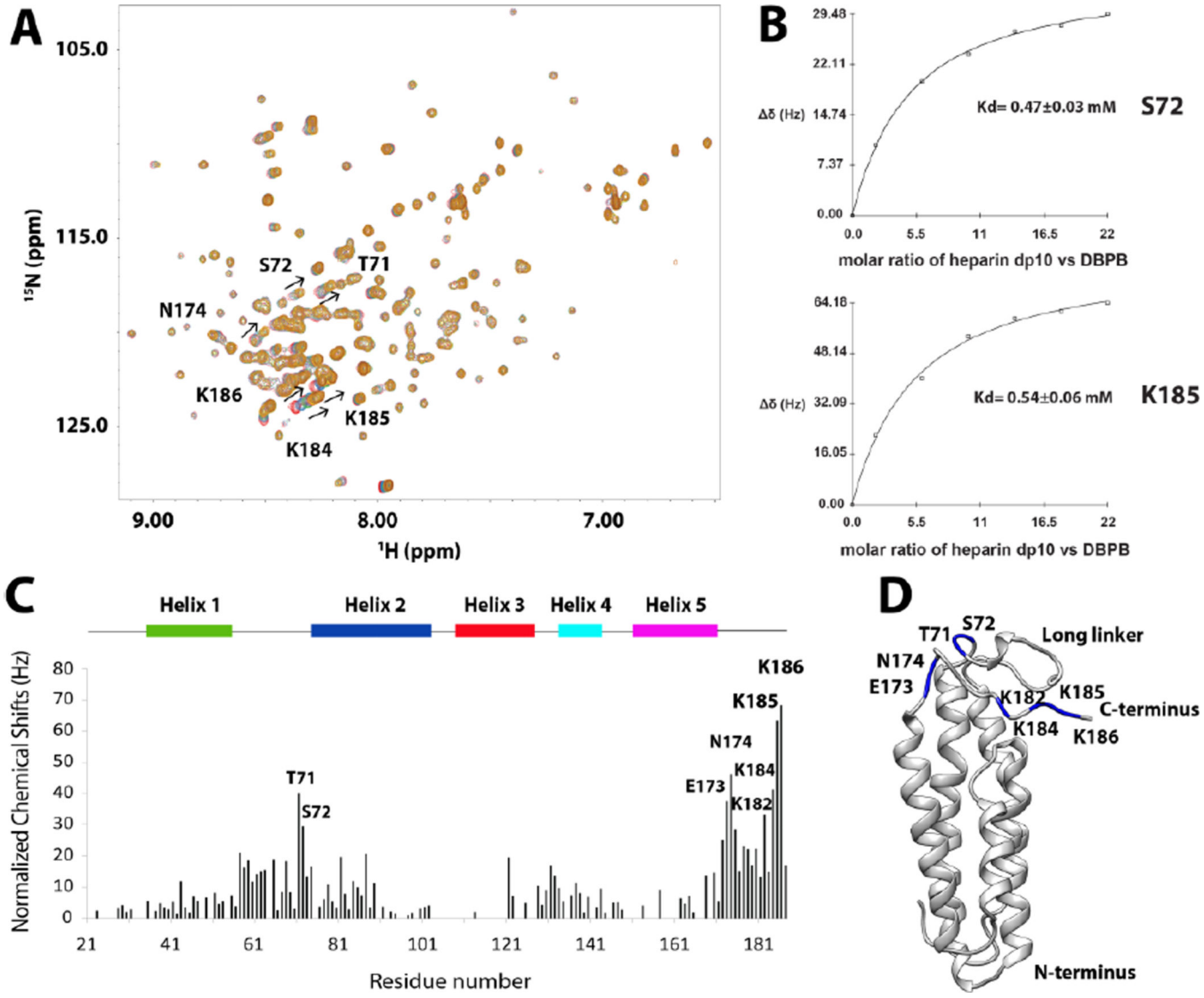

Figure 6. DBPB titration with heparin dp10

(A) ^{1}H-^{15} N HSQC overlays of WT B31 DBPB with increasing concentrations of heparin dp10. Signals with large migrations are labeled with their residue numbers and arrows to indicate migration directions. T71, S72, E173, N174, K182, K184, K185 and K186 have the largest migration. Contours are color-coded with increasing concentrations of heparin dp10 (0, 0.2, 0.6, 1.0, 1.4, 1.8 and 2.2 mM). (B) Binding curves of DBPB residues S72 and K185 when titrated with heparin dp10. (C) Residue specific heparin-induced chemical shift changes. Normalized chemical shift perturbations to backbone amide nitrogen and proton by heparin dp10 are displayed. (D) Ribbon conformer of DBPB in the same orientation as in Figure 4B with residues showing large perturbations colored blue.

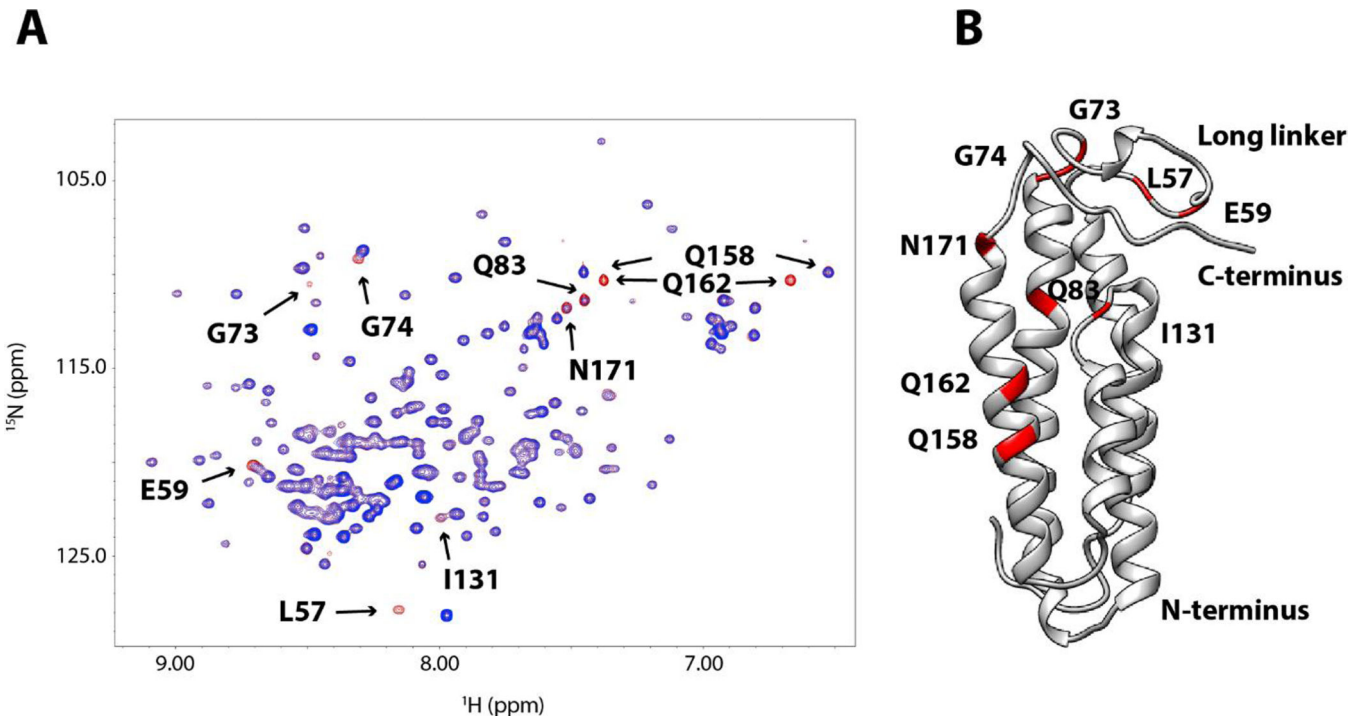

Figure 7. PRE perturbation of DBPB by paramagnetically labeled DS dp12

(A) ^{1}H- ^{15} N HSQC overlays of WT B31 DBPB with 8 molar equivalents of TEMPO-labeled DS dp12. HSQC spectrum before the radical is reduced is shown in blue. HSQC spectrum of the protein after reduction of the radical is shown in red. Residues showing prominent PRE perturbations are indicated. They are L57, E59, G73, G74, Q83, I131, Q158, Q162 and N171. (B) Ribbon representation of DBPB in the same orientation as in Figure 4B with TEMPO-perturbed residues colored red.

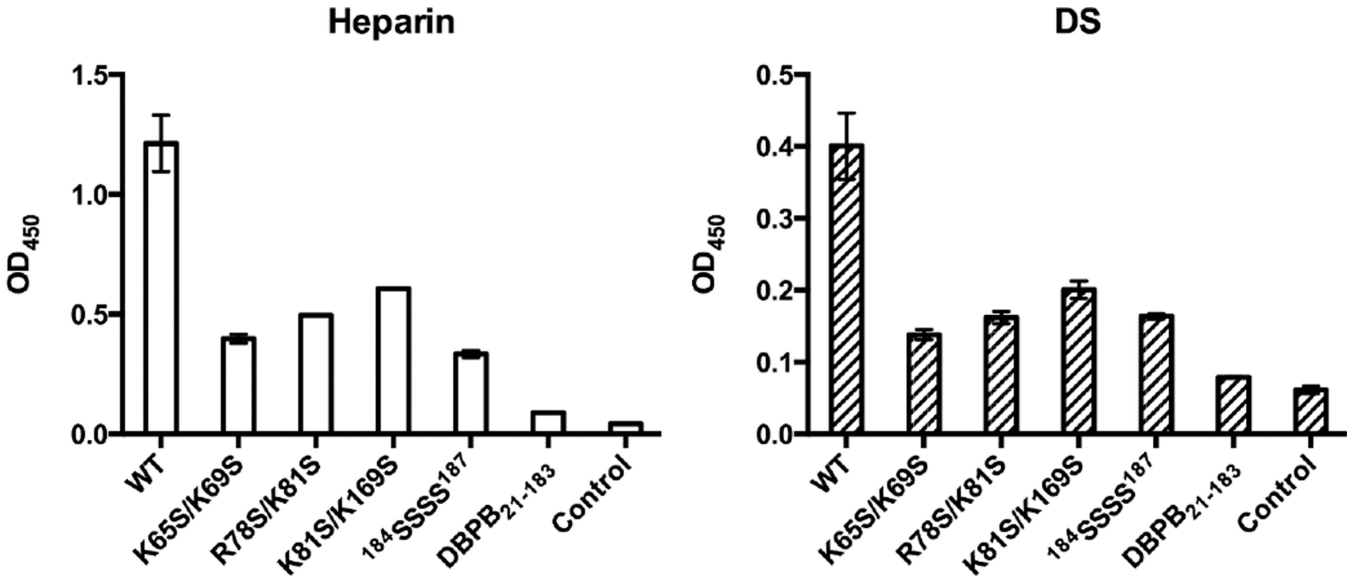

Figure 8. Impact of mutations on DBPB's heparin and DS affinities evaluated using immobilized heparin or DS ELISA

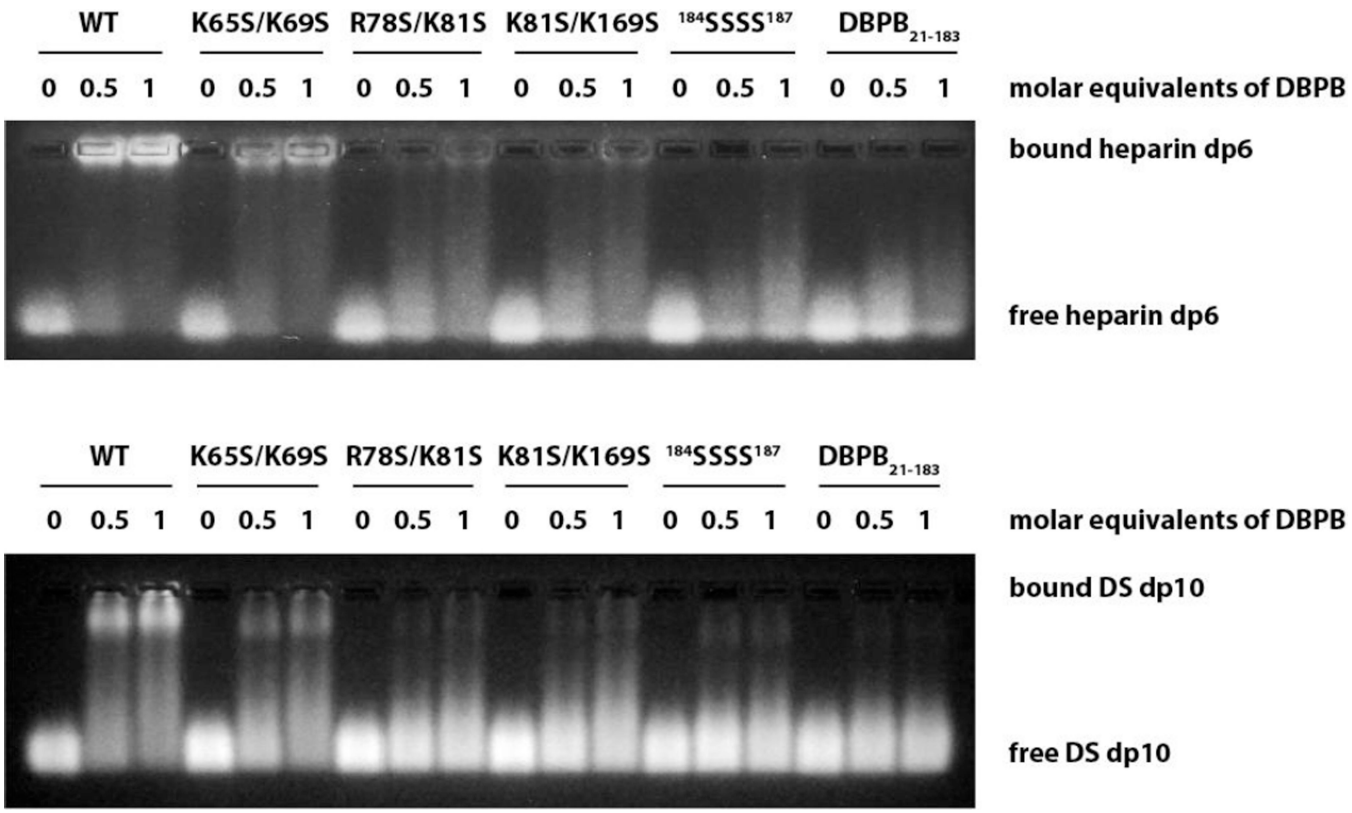

Figure 9. GMSA evaluation of the effects of mutations on DBPB's heparin and DS affinity

Table 1
Structural statistics for the ensemble of DBPB structures

no. of NOE-based distance constraints	
total	1635
intra-residue (i=j)	484
sequential (|i-j|=1)	477
medium range (1<|i-j|<5)	389
long range (|i-j|≥5)	285
NOE constraints per restrained residue [a]	10.0
no. of RDCs	
H-N	93
N-C	91
no. of dihedral angle constraints	240
total no. of structures computed	50
no. of structures used	10
constraint violations [b]	
no. of distance violations per structure	
0.1~0.5 Å	37
>0.5 Å	0.9
no. of dihedral angle violations per structure	
>10°	0.5
no. of RDC violations per structure	
>1 Hz	1.4
RMSD	
all backbone atoms	0.7 Å (ordered [c])
all heavy atoms	1.2 Å (ordered [c])
Ramachandran plot summary from Procheck [d] (%)	
most favored regions	92.4
additionally allowed regions	7.4
generously allowed regions	0.2
disallowed regions	0.0

[a] There are 161 residues with conformational restricting constraints.

[b] Calculated for all constraints for the given residues, using a sum over r^{-6}.

[c] Residues 34–54, 74–103, 108–128, 134–143, and 150–171.

[d] Residues 30–57, 67–69, 75–130, 134–144, and 150–170.

Table 2

Kd of DBPB's interactions with GAG fragments

WT and mutant DBPBs were titrated with heparin dp10 and DS dp10. Kds were calculated based on S72 and K185 for DBPBs.

	S72 (mM)	K185 (mM)
WT	0.47 ± 0.03	0.54 ± 0.06
K65S/K69S	0.90 ± 0.12	0.88 ± 0.06
R78S/K81S	1.04 ± 0.26	1.16 ± 0.18
K81S/K169S	1.24 ± 0.35	1.22 ± 0.12
^{184}SSSS^{187}	-------	-------
DBPB$_{21–183}$	-------	-------